


RESEARCH ARTICLE OPEN ACCESS

Textile Actuation Based on In-Air Actuating Polypyrrole-Based Tape Yarns for Wearable Soft Robotics: Toward On-Body Applications

Carin Backe¹ | Jose G. Martinez² | Li Guo¹ | Edwin W. H. Jager² | Nils-Krister Persson^{1,3} 

¹The Swedish School of Textiles, Polymeric E-Textiles, University of Borås, Borås, Sweden | ²Department of Physics, Chemistry and Biology (IFM), Sensor and Actuator Systems, Linköping University, Linköping, Sweden | ³Smart Textiles Technology Lab, Smart Textiles, University of Borås, Borås, Sweden

Correspondence: Nils-Krister Persson (nils-krister.persson@hb.se)

Received: 31 October 2025 | **Revised:** 30 January 2026 | **Accepted:** 18 February 2026

Keywords: conjugated polymers | electromechanically active polymers | in-air actuation | soft actuators | textile fabric actuators

ABSTRACT

Soft robotics employs deformable materials and structures to achieve compliance and adaptability, enabling safe and close interaction with humans. Merging electromechanically active polymer actuation with textile technology enables soft, large area actuators with form factors being 1D (fibers), 2D (fabrics), or 3D (garments), all relevant for wearable soft robotics. This study investigates in-air actuating polypyrrole (PPy)-based trilayer tape yarns (TYs) and the effect of integrating them into woven fabric actuators. Individual TYs are developed, consisting of two polypyrrole layers sandwiching a poly(vinylidene fluoride) (PVDF) membrane filled with anionic liquids (IL). The impact of ionic liquid, PPy thickness, and frequency response on displacement and blocking force is investigated. Individual TYs offer the highest displacement of 30.6 ± 3.6 mm (± 1.5 V) at 2.5 mHz and blocking force at 0.20 ± 0.07 mN (± 1.0 V, 2.5 mHz). Next, weaving is used to integrate TYs into plain weave actuating fabrics, enabling the assembly of many TYs together without a decrease in displacement. Additive force in woven actuators scales linearly with increased force up to 1.13 ± 0.18 mN (5 TYs), addressed by integrated conductive yarns. Multiarea fabric actuation is demonstrated, as well as an on-body wearable application of the fabric actuator.

1 | Introduction

Soft robotics is a flourishing direction for robotics research where deformable materials and structures are used to achieve compliance and adaptability, opening up for close-to-human usage [1–3]. Soft robotics typically requires *soft actuators* that need to both exert force and be capable of conforming to the environment, whether it is in robotic-human interfaces or in the manipulation of fragile objects [4]. Hence, wearable soft robotics requires mechanical flexibility, compliance matching, low weight, biocompatibility, and the ability to control actuation (actuation-on-demand such as electrical steering rather than actuation-by-chance such as relying on ambient heat) [5]. Textiles and textile processes offer several advantages that make them suitable for developing soft actuating systems [6]. Textiles are

omnipresent in modern daily life, in many forms such as clothing, interior products, and technical applications. Among these, garments represent one of the most familiar textile products, as they are used daily and remain in constant contact with the human body, thus being the wearable par excellence [7]. Textile processes are capable of assembling a range of materials with different properties in intricate patterns into flexible structures, giving textile fabrics an inherent softness as well as in-plane complexity. In this way, textiles exhibit high conformability and can adapt to the complex geometries and curvatures of the human body. Thanks to this adaptability as well as matched hardness values of tissue and textiles, a soft actuator made of textile redistributes forces over the wide contact area of the skin, avoiding puncture in the soft actuator as well as in the skin [8]. They are also breathable and

This is an open access article under the terms of the [Creative Commons Attribution](https://creativecommons.org/licenses/by/4.0/) License, which permits use, distribution and reproduction in any medium, provided the original work is properly cited.

© 2026 The Author(s). *Advanced Robotics Research* published by Wiley-VCH GmbH.

lightweight, while mechanically capable of handling external loads. These characteristics make textiles uniquely positioned as a platform for creating wearable soft robotics [9].

Electromechanically active polymers (EAPs) generate motion and change shape through electrical stimulation. It is a promising category of materials to fulfill the requirements of soft robotics of controlled actuation; being independent on fluctuating temperature or moisture content; body proximate actuation thanks to low currents and low power consumption; and themselves being of polymeric nature compatible with curved form factors. One class of EAPs, conducting polymers (CPs), can be used as soft actuators when paired with an electrolyte or ionic liquid and under an applied voltage. The underlying actuation mechanism is a reversible volume change due to electrochemically induced redox reactions, where the polymer becomes positively or negatively charged, and a mass transfer occurs due to ions entering from the surrounding ion source to maintain electroneutrality [10]. CPs, such as polypyrrole (PPy), are soft materials which can be processed into thin films and only require low voltages (1–5 V) to operate [11, 12]. However, they typically require liquid electrolytic environment for operation which is limiting for wearable applications [10, 13]. As they are usually obtained in thin films, they also produce relatively small forces [14]. It is therefore of interest to scale up the exerted force. A strategy is to assemble several actuators in parallel and serial constellations. It is also of interest to decouple the dependence between EAP actuation and liquid electrolyte. An actuating system with a solid electrolyte is preferable for in-air applications. Most studies of EAP actuation in relation to textiles have been performed by coating on ready-made fabrics, which is an effective method but obfuscates important textile parameters [15, 16]. Furthermore, it reduces the comfort of the fabric actuators. Therefore, the development of actuating tape yarns (TYs) is crucial to study the impact of textile integration into fabrics, circumventing these issues related to coatings. For this, a strategy for making an actuating trilayer yarn structure based on gel with inclusion of ionic liquid, IL, has been tested in a feasibility study [17]. In order to hinder degradation and to make a more robust TY, another strategy is here developed, incorporating the IL in a porous membrane creating a reservoir of ions.

The fundamental *textile hierarchy* for textiles presents great flexibility in designing actuating structures. Functionality can, not only on the polymeric level, be added on a A) yarn, B) fabric, or C) garment level. Furthermore, the mechanical properties can be tuned at each level by the combination of materials and construction. It is also the case that all levels in the textile hierarchy have interesting actuation applications. Single yarn actuators from level A) could find use in minimally invasive neurosurgery; as for neuroendoscopy, fabric actuators have a widespread use as adaptive filters and topology switching surfaces; and for level C), a wealth of garments for haptic communication active orthoses, morphing, etc., are possible [18–22]. For B) and C), a challenge is to achieve integrated control and incorporate powering components, to make it a stand-alone device. Textile yarns can exhibit different functions, such as actuating, sensing, or conducting. Furthermore, passive structural yarns offer both mechanical stability and comfort properties which are beneficial for wearables. By integrating these functions directly into a fabric structure during fabrication, textile-based soft robotics can be created. Such textile systems enable actuation with maintained

compliance and conformability and potentially making textile materials and textile processes a very valuable tool for the soft actuator community.

This study is organized as follows. Following the membrane strategy, we developed actuating TYs of CPs which can operate in-air and withstand the mechanical distress during textile processes. The concept of using poly(vinylidene fluoride) (PVDF) membranes with thin Au layers and deposited PPy to create trilayer actuators was already developed for actuators in the μm scale; however, for integration in macroscopic textile fabrics, yarns on a larger scale are required [23–25]. The procedure was therefore adapted in order to obtain longer TYs that are more compatible with the weaving process. The synthesis and characterization of individual CP-based TYs is studied, including the impact of layer thickness, electrolyte, ionic liquid, voltage, and frequency. Secondly, a yarn-level integration scheme into fabric actuators was employed, addressing level B in the textile hierarchy. Weaving is an additive manufacturing process in which small individual components (here TYs) are assembled together. Also passive, non-actuating yarns are used. This preserves the inherent pliability and conformal ability of fabrics while simultaneously enabling the investigation of integration on actuation performance. Actuation performance both in terms of force and deformation is investigated. We finalize with addressing level C by showing a textile-based haptic communication device.

2 | Soft Actuators Using CPs + Textiles

2.1 | Polypyrrole Trilayer TYs

Actuating yarns are a key functional element to obtain actuating fabrics [26, 27]. Here, we developed trilayer TYs based on the electroactive polymer PPy that can move in air due to the storage of an electrolyte in a PVDF membrane. The TYs consist of a commercially available PVDF membrane coated on both sides with a thin layer of Au, and on top of those 2 thin layers of gold, the electromechanically active PPy layers. When PPy is polymerized in the presence of large ions like dodecylbenzenesulfonate (DBS⁻), these will get trapped in the polymer matrix [28]. When the PVDF membrane is soaked with an electrolyte, it is then possible to reversibly oxidize and reduce the PPy layers, producing the swelling or shrinking of these two layers. When a potential difference is applied between the two PPy layers, one of them will be oxidized, i.e., positive charges will appear along the polymeric chains, and the other one will be reduced, i.e., positive charges will disappear along the polymeric chains. In order to compensate for the new electrical state and maintain electroneutrality, ions (cations in this case) exit or enter the PPy layers. Such exchange of ions promotes the shrinking or swelling of the PPy layers. The swelling layer will push the trilayer while the shrinking layer will pull the trilayer, producing a bending movement (Figure 1), making it possible to obtain bending TY actuators. When the polarity is reversed, the swollen layer will start to shrink and the shrunken layer will start to swell, reversing the direction of the movement.

2.2 | Fabricating Woven Actuators

Weaving is an appropriate method for integrating TYs into woven structures, when taking their geometry, short dimensions,

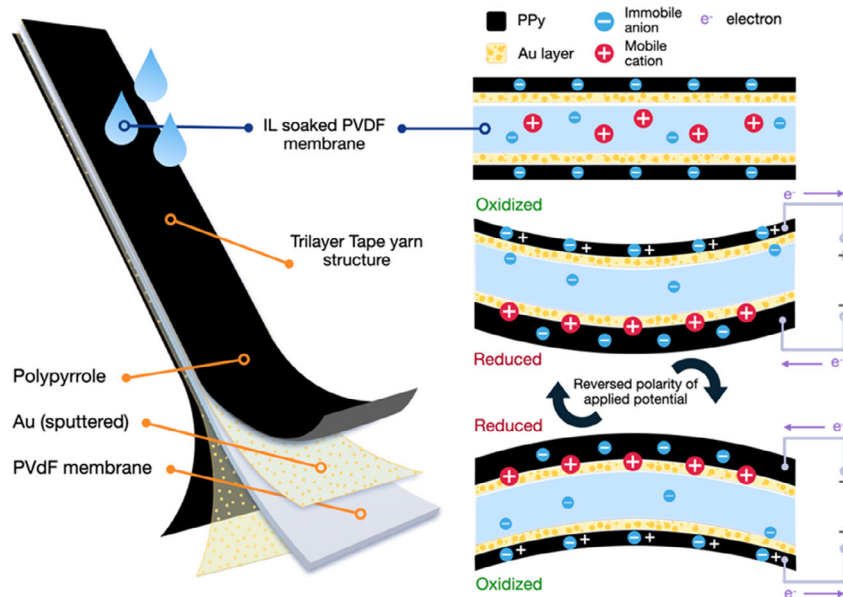


FIGURE 1 | Polypyrrole trilayer TY. The actuation mechanism relies on the mass transfer of ions in and out of the polymer due to electrochemically induced redox reactions when a voltage is applied.

and mechanical properties into consideration. Woven structures consist of, generally, two yarn systems called warp and weft. Each system is a parallel organization of warp yarns that are perpendicularly interlaced with weft yarns to form a large, grid-like fabric structure. Our integration strategy introduced TYs as weft yarns and passive nonactuating yarns in the warp (Figure 2) that enable the processing of small independent TY actuators into an interconnected actuating fabric structure.

2.2.1 | Woven Actuator Concept

Fabrics typically span large areas, using kilometers of yarns, for a wide range of applications. To evaluate the behavior of woven

actuators containing TYs, which in this study were considerably shorter than conventional yarns, smaller woven actuator *segments* were created. These representative woven actuator structures enabled the investigation of bending displacement and force on a fabric level. A typical actuator segment consisted of 5 TYs surrounded by passive nonactuating polyester (PES) yarns in 5 mm weft-zones on each side to ensure maintained fabric integrity. The number of TYs (5) was chosen as the standard number of integrated TYs in a segment to mitigate any individualities between yarn performance and to achieve more uniform behavior of fabric actuator samples. Weaving allows for the parallel assembly of yarns which has previously been found to amplify the force output of fabric actuators [15, 17]. By

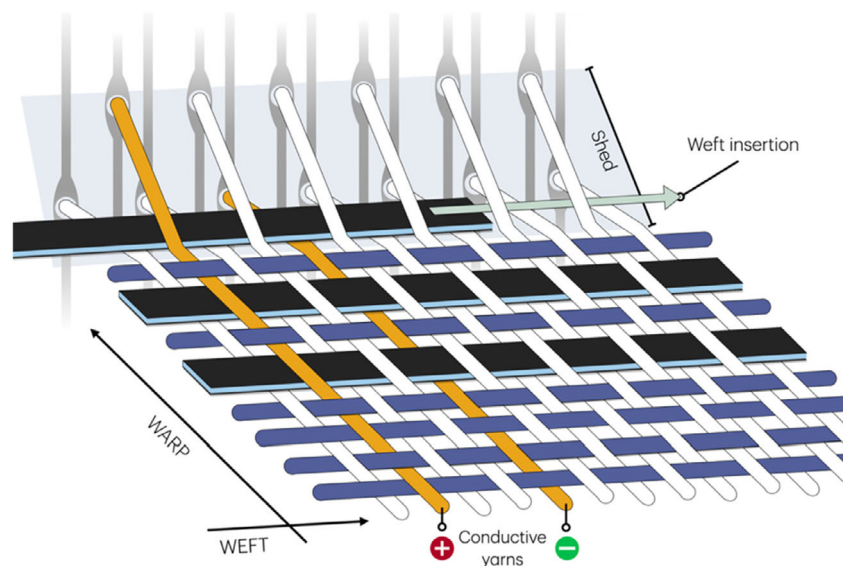


FIGURE 2 | Weaving process of fabric actuators. Warp threads are separated (lifted) into a shed by the control of shafts in a predetermined pattern. The weft yarns are inserted in the shed perpendicular to the warp yarns and create a parallel assembly of TYs. Electrical connection to the TYs can be achieved by integrating two conductive yarns, substituting two passive warp yarns in the threading of the weaving loom. These act as positive and negative poles, switching polarity when the voltage direction is reversed.

integrating multiple TYs into a woven configuration, this effect could be investigated for in-air actuating woven structures too. The combination of several weave segments can create a larger area of actuation, and this can be accomplished by weaving multiple segments in parallel and/or serial assemblies (Figure S1). However, electrical connection and TY control are essential. CP films are typically addressed directly by conductive clamps. This enables stable connections but also mechanically fixates the actuators in place. Using weaving, electrically conductive yarns can be used to fully integrate this function into the same fabric during the same weaving process, thus removing the need for a rigid clamp while preserving fabric properties such as flexibility. This is a crucial step toward untethered, free-standing fabric actuators, a critical aspect for wearability purposes and soft robotic applications and production economics [29]. The grid-like structure of woven constructions enables the purposeful replacement of certain nonactuating warp yarns with conductive yarns (Figure 2) [17]. By correct placement in the warp direction according to the sequence of weaving pattern, connection to TYs is achieved, and electrical stimuli can be given to integrated TYs without external clamping of the samples.

3 | Results and Discussion

To demonstrate the concept of woven actuation, the TYs were first characterized individually, then integrated into woven structures, and evaluated on a fabric level, similar to our previous work with in-air actuating weaves [17].

3.1 | Individual TYs

In this work, we explored the possibility of obtaining longer TYs based on trilayer polypyrrole/polyvinylidene fluoride/polypyrrole (PPy/PVDF/PPy). The yarns should be of proper size to be processable into fabrics and have suitable mechanical properties to withstand the mechanical stress during weaving. To achieve cm-scale TYs, larger pieces of PVDF membrane ($11 \times 8 \text{ cm}^2$, limited by the size of the vacuum chamber and holder of the sputter) were first sputtered with Cr and Au, obtaining a uniform coating (Figure S2A). Next, we electropolymerized PPy on both sides of the PVDF membrane, obtaining a

PPy/PVDF/PPy trilayer. By electropolymerizing on the big piece directly, it was not possible to obtain a uniform PPy coating, as could be seen optically (Figure S2B). This could be due to the low conductivity of the thin Au coating. Thus, the large pieces were cut into 4 smaller pieces and electropolymerized with PPy, resulting in a much more uniform coating (Figure S2C). The electropolymerization was performed by applying a constant potential of $+0.6 \text{ V vs. Ag/AgCl (3M NaCl)}$ for the time required to consume a specific charge (typically 40 C for the $5.5 \times 3.5 \text{ cm}^2$ piece of Au-coated PVDF immersed in the electropolymerization electrolyte, resulting in an average consumed specific charge of 1.04 C/cm^2 , taking into account that the electropolymerization occurred simultaneously on both sides). The current increased quickly during nucleation and coalescence until it reached a plateau with a slow decrease over time (Figure S3A) [30]. This decrease could indicate partial loss of conductivity for thicker PPy films, as PPy has a lower electrical conductivity than Au [31]. Thereafter, the borders were cut to avoid shortcuts between the two sides, due to the synthesis procedure, and $50 \times 3 \text{ mm}$ long TYs (Figure S2D) were cut from the remaining film. Finally, PPy/PVDF/PPy TYs were immersed in the used electrolyte overnight and left to dry for 3 h before use. The electroactivity of the TYs was then examined by cyclic voltammetry (Figure S3B). It was possible to observe clear oxidation and reduction peaks, pointing to a successful deposition of electroactive PPy [32].

The obtained TYs were then actuated to check their performance by applying symmetrical square potential waves, and their actuation was studied through video recording of the movement. Figure 3A shows the current passing through the TY actuator for the first 10 actuation cycles. The current showed an initial peak in each half cycle after which it decreased. It is also possible to observe how the peak is increasing, especially during the first cycles. Figure 3B shows the displacement of the tip of the TY measured from the frames of the video recorded during the actuation. It was possible to observe how the tip moved toward the left side (considered here as negative) during reduction of the right side of the TY and simultaneous oxidation of the left side and toward the opposite right side (considered here as positive) when the potential was reversed, due to the oxidation of the right side of the TY and simultaneous reduction of the left side. As in the case of the peak current, which increased with the number of cycles, the actuation followed a similar trend, obtaining a bigger

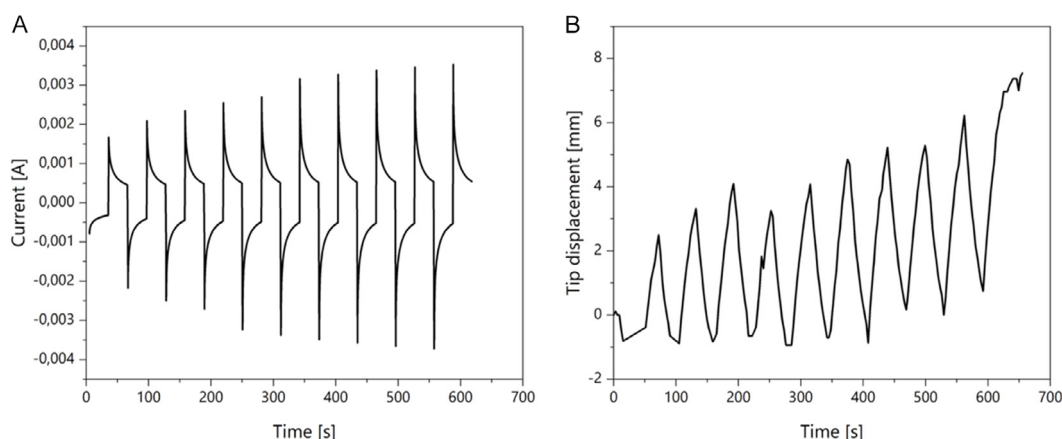


FIGURE 3 | (A) Chronoamperograms obtained from a PPy/PVDF/PPy TY when a square potential wave of $\pm 1.0 \text{ V}$ kept each potential for 30 s, and (B) displacement of the tip of the PPy/PVDF/PPy TY during the chronoamperograms shown in (A).

actuation for later cycles. This points to the Faradaic nature of the actuation: PPy is swelling and shrinking due to the insertion or expulsion of ions and solvent from the electrolyte present in the PVDF membrane. When a larger charge (more current) is consumed, additional ions can be inserted into the polymer matrix, leading to a larger displacement [33].

3.1.1 | Ionic Liquid/Electrolyte

To optimize the actuation, different electrolytes were investigated. After electropolymerization and drying, PPy/PVDF/PPy TYs were soaked in 3 different electrolytes: 2 ionic liquids (choline acetate and 1-ethyl-3-methylimidazolium bis(trifluoromethylsulfonyl)imide, EMIMTFSI) and 0.1 M lithium bis(trifluoromethanesulfonyl)imide (LiTFSI) dissolved in propylene carbonate (PC). After letting the excess dry for 3 h, we actuated the single TY by applying symmetrical square potential waves of ± 1.0 V, keeping each potential for 30 s, while recording the video of the actuation. The displacement of the tip can be seen in Table 1. The largest displacement was obtained in choline acetate. A large variability was seen when using 0.1 M LiTFSI in PC, where one sample was comparable to the actuation performance of those moved in choline acetate, while the other two samples actuated a lot less. Actuation in EMIMTFSI showed the smallest displacement. These results are in agreement with previous results: the electrolyte (both ions and solvent present) plays a crucial role on the actuation [34–36]. Besides, the interaction between choline acetate and water could have a positive effect [37, 38]. The solvent also plays a key role in the actuation of

conducting polymers, and the incorporation of water could boost their actuation [39, 40].

3.1.2 | Different PPy Thickness

Another variable that has an important influence on the actuation is the thickness of the PPy coating [41]. It is possible to obtain different PPy thicknesses by consuming different amount of charge during the electropolymerization [42–45]. Thus, we electropolymerized PPy until different charges were consumed (20, 40, 60, and 80 C) and the actuation of the TYs was analyzed. Figure 4A shows the average actuation of the TYs obtained by the consumption of different electropolymerization charges. It is possible to observe how the maximum displacement was obtained by consuming 40 C during electropolymerization, although the differences were not significant with thinner (20 C) or thicker (60 C) films. For even thicker PPy coating, the displacement decreased substantially to almost zero actuation. This could be due to the changes in the mechanical properties of the different layers (in this case mostly the PPy layers), affecting the performance [41]. It has been observed that thicker PPy layers are less electroactive in comparison to thinner ones relative to their initial thickness. That, together with the fact that thicker PPy is also stiffer, substantially affects the performance [43].

The blocking force produced by the tip of the PPy/PVDF/PPy TY actuator was also measured. Figure S4 shows the force evolution measured for PPy/PVDF/PPy TY (40 C electropolymerization of PPy) by applying square potential waves of ± 1.0 V, each potential kept for 60 s. It is possible to observe how the force increases during the first half cycle and decreases when the potential is reversed, getting a stable response over the cycles. For different PPy thicknesses, it is possible to observe how the average force increased up to 60 C polymerized PPy/PVDF/PPy TY actuators, then showed forces around 0 for a PPy/PVDF/PPy TY actuator obtained by consumption of 80 C (Figure 4B). It is worth noting that the standard deviation of the measurements, especially for the thinnest PPy (20 C consumed charge), was quite large, making the differences in force not significant. Besides, such a small force measured for the thicker PPy produced noisy measurement data due to the produced force being small and close to or under

TABLE 1 | Displacement obtained by tape PPy/PVDF/PPy TYs after soaking them in different ionic liquids/electrolyte.

Ionic liquid/electrolyte	Displacement
Choline acetate	12.1 ± 4.4 mm
EMIMTFSI	1.4 ± 0.5 mm
0.1 M LiTFSI in PC	4.2 ± 5.1 mm

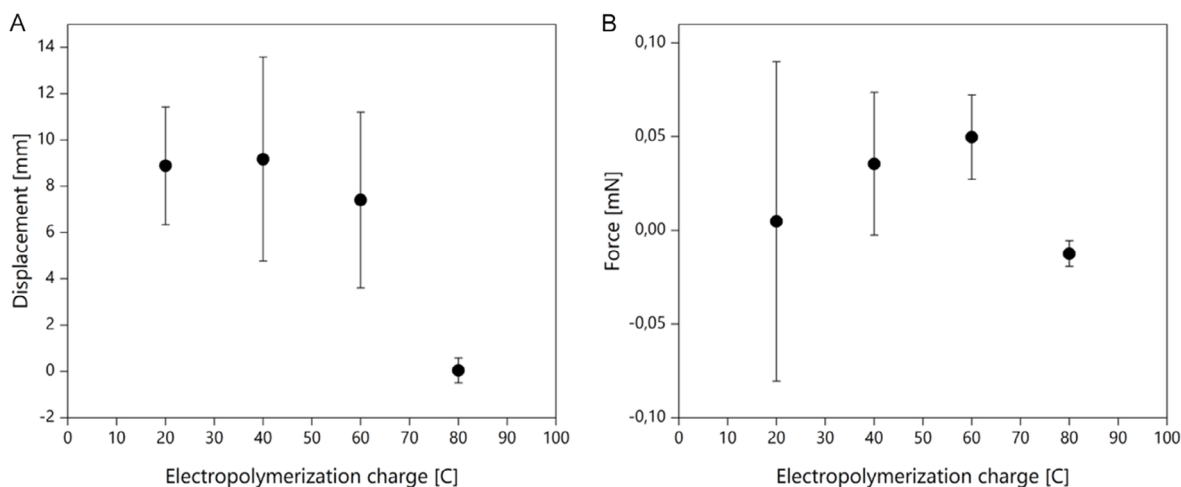


FIGURE 4 | Measurements at the tip of a PPy/PVDF/PPy TY obtained by consumption of different electropolymerization charges (20, 40, 60, 80 C). Displacement (A) was captured during applied square potential waves of ± 1.0 V when each potential was kept for 30 s, and force exerted (B) when each potential was kept for 60 s.

the detection limit of the lever arm used to perform the measurement and presented a small nonreversible drift. Based on these results, 40C-PPy/PVDF/PPy TY actuators were chosen for the weaving studies, as they gave the largest tip displacement and one of the largest forces.

3.1.3 | Frequency Response

Both the speed of movement and the maximum amplitude of movement that can be achieved for different actuation times are also relevant for practical applications, where different time scales might be needed. Thus, we studied the frequency response of individual PPy/PVDF/PPy TY actuators (Figure 5).

It is possible to observe how, for high frequencies (higher than 0.05 Hz), the actuation is quite limited for both the displacement (Figure 5A) and the exerted force (Figure 5B). This is due to the fact that the time available for diffusion of ions and solvent through the PPy film is limited, so the amount of ions and solvent molecules that can be exchanged (and thus produce movement) is limited [46]. For lower frequencies, both the force and displacement increase when the frequency decreases up to 0.005 Hz. Longer time allows more ions and solvent molecules to be incorporated to (or expelled from) the PPy film producing the movement [11]. By increasing the potential, it is possible to observe, especially in the case of the tip displacement, how a higher potential results in a larger actuation in that region. A higher electrochemical energy allowed for a larger amount of ions and solvent exchanged. For even lower frequencies, the actuation seems to decrease slightly.

3.1.4 | Lifetime of Individual TYs

Another important aspect for practical applications is the lifetime of the TY actuators. Figure 6 shows the average displacement during consecutive cycling up to 1000 cycles, at different symmetrical square potential waves (1.0, 1.5, and 2.0 V). The results show how displacement increased during the first cycles for all applied potentials, which is probably related to the increase in the consumed charge, also observed in Figure 3. After 160 cycles, the displacement started to decrease. For the highest applied potential (± 2.0 V), this decay was more pronounced, with displacement

decreasing at a higher rate. When a potential of ± 1.5 V was applied, the decline occurred in a similar way but at a slower rate. When a low potential (± 1.0 V) was applied, the movement was smaller in all cases, but more uniform at the end between the different potentials.

3.2 | Behavior of Woven Actuators

Two types of woven segments were produced, as seen in Figure 7A. The first enabled direct stimulation by Kelvin electrode clamps, while the second relied on integrated conductive yarns to address TYs directly in the weave. The weaving process must be adequately adjusted for the mechanical properties and sensitivities of the TYs. To avoid folding and subsequent breakage, the TYs are inserted in the weft direction manually. During the weaving process, two critical aspects are (1) the force at which the weft insertion is beaten into position in the shed (beat-up force) and (2) the warp tension. The beat-up force is required for correct placement; however, too high force causes the TYs to break in a lengthwise direction, folding over itself inside the shed. Warp tension is adjusted to allow the weaving of a plain weave structure. At too high warp tension, a significant force is exerted onto the TYs during the next shed formation (preparing for the next weft insertion), causing the TYs to snap. It is important to consider the impact of integrating TYs into fabric actuators on actuation performance; therefore, the displacement and blocking force behavior of plain weave actuator segments were evaluated. The fabric actuators were then increasingly complex, with the integration of conductive yarns for TY control and multiple segments in either parallel or serial configurations. Individual TYs were benchmarked from the same batch (Figure S5) prior to studying woven actuation.

3.2.1 | Bending Displacement of Woven Actuators

The woven structure is often described by its relatively rigid properties, compared to knitted structures. It is thus of interest to evaluate the impact of woven integration on the displacement behavior of TYs, determining if the woven structure negatively impacts the range of displacement possible. Single segments of woven actuators showed similar displacement profiles, as seen

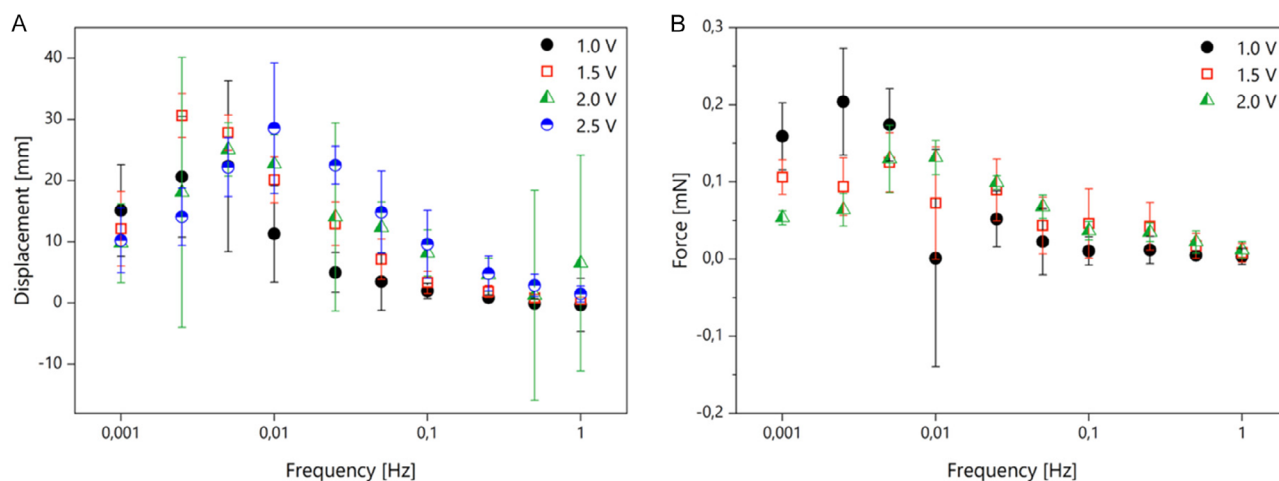


FIGURE 5 | Frequency response of (A) displacement of the tip or (B) force produced by the tip of individual PPy/PVDF/PPy TYs after applying symmetrical square potential waves of different potentials.

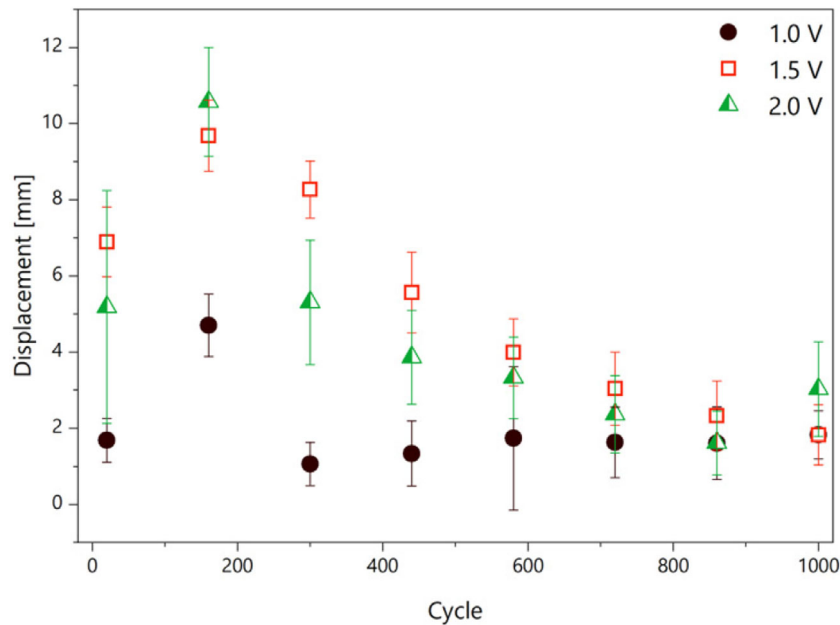


FIGURE 6 | Evolution of the average displacement of the tip of individual PPy/PVDF/PPy TYs after applying three different symmetrical square-wave potentials, each of them kept for 60 s, for up to 1000 cycles.

in Figure 7B with average displacements ranging between a minimum of 3.7 ± 0.10 and a maximum of 5.0 ± 0.07 mm between the three samples. The average displacement was 4.11 ± 0.26 mm, which is on the same level as nonintegrated TYs of the same batch and measured at the same frequency. Higher displacements were recorded for individual TYs at lower frequencies, as previously shown in Figure 5. Lower frequencies correlated to higher displacements due to factors related to the ion diffusion mechanism. At lower frequencies, ions have more time to enter the CP layers, resulting in larger expansions, while the opposite is true for higher frequencies. Samples with integrated electrical connections exhibited displacements in the same or better capacity than externally clamped woven actuators.

3.2.2 | Blocking Force and Additivity of Woven Actuators

The woven segments were evaluated by the blocking force registered at the tip of the sample as it is clamped in a vertical position. While the maximum blocking force is of interest, i.e., when all 5 TYs are active, so was the additivity of force by using different numbers of active TYs in the same segment. Additivity of force was measured using two approaches. The first used woven segments with 5 TYs where each TY was electrically and mechanically clamped by a separate Kelvin clamp, using a specialized clamp-setup containing 5 pairs of Kelvin clamps. The TYs were then individually and sequentially stimulated in a set order. TYs were stimulated one at a time starting from the middle and continuing outwards, measuring blocking force at each additional active TY. The sequential scheme can be found in Figure S6. The second approach was built on making smaller woven segments, each with different number of integrated TYs. These were designated into units, where each unit contained 1 TY and necessary nonactuating weft yarns to facilitate fabric integrity. In this way, woven segments with increasing number of units containing TYs were created (1–5 TYs) (Figure S7). In contrast to the previous approach, all TYs were always active within

the same sample. The results of the two approaches are found in Figure 7B,C, respectively. Comparing the blocking force of a single, nonintegrated, TY (0.1 ± 0.04 mN) to 1 active TY in both scenarios reveals an increase to 0.66 ± 0.28 mN (Figure 6C) and 0.44 ± 0.10 mN (Figure 6D). The force then continues to increase up to 5 actuating TYs, showing forces at 1.07 ± 0.16 mN (Figure 6C) and 1.13 ± 0.18 mN (Figure 6D). The higher degree of variability in 5-TY segments, which are activated sequentially, is most likely due to the changing degree of stiffness inside the fabric. As some TYs are inactive, their higher stiffness, compared to passive nonactuating weft yarns (polyester), causes the overall fabric stiffness to change depending on the number of active TYs in the weave. The woven segments built on TY units exhibit a more linear relationship between the number of active TYs and blocking force output.

3.3 | Multisegmented Woven Actuators

3.3.1 | Parallel Assembly

We have previously explored the idea of fabrics with multiple areas independently actuating, where a fabric actuator exhibits either uniform bending motion or independent motion patterns [17]. Here, parallel assembly was further investigated concerning the influence of passive weft zones. A two-segment fabric actuator was created, separated by a 10-mm passive nonactuating weft zone. Initial testing of the displacement behavior was conducted by placing the fabric actuator perpendicular to the laser, with the measurement area positioned in a horizontal direction across the measurement points 1, 2, and 3 on the fabric, as seen in Figure 8A. The fabric actuator bends and its displacement is measured in the Z-direction inside this laser field. After completing 10 cycles of actuation, the passive weft yarns in the middle weft zone were removed (marked red in Figure 7A). The fabric actuator was tested again, showing on average a 38.5% increase in displacement across the entirety of the fabric actuator (Figure 8B).

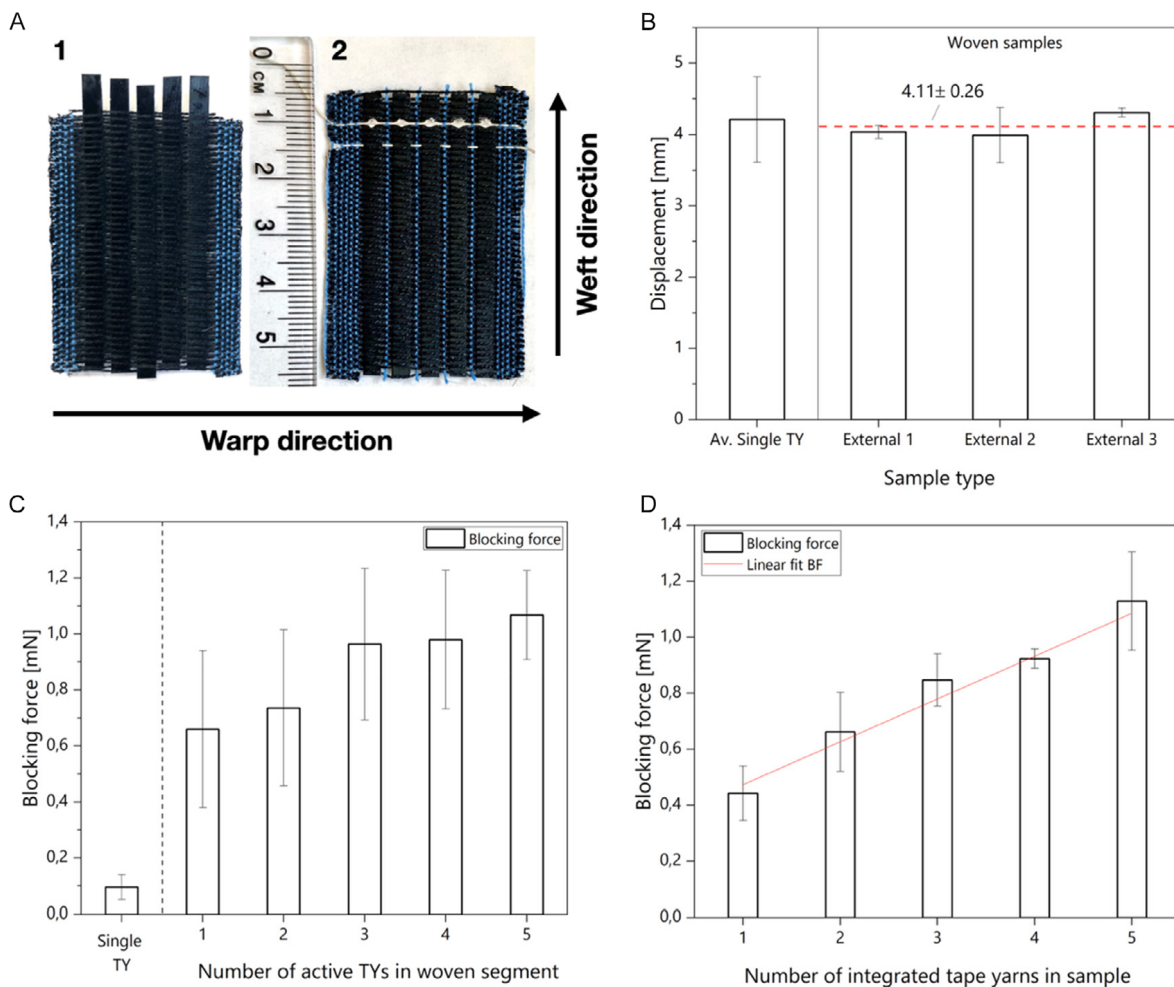


FIGURE 7 | Displacement and blocking force of woven actuator segments. Woven samples stimulated by external electrode clamps or integrated conductive yarns were produced (A). (B) shows displacement of three A1 samples consisting of five PPy TYs, each compared to the average single TY displacement (same batch). (C) shows the blocking force of woven actuators, when sequentially activating the integrated TYs and (D) linear increase in force (R^2 0.969) for woven segments containing different numbers of integrated TYs. Three replicates were tested, each at $\pm 2V$ applied potential at 30s intervals for a total of 10 complete cycles.

The effect is most likely influenced by both structural textile parameters and individual performance of TYs.

3.3.2 | Serial Assembly

Woven segments can also be connected in a serial configuration. In this case, the segments are mechanically and electrically separated, and the fabric is connected through nonactuating weft yarns. The assembly consisted of segments A, B, and C and clamped mechanically at the top above segment A. Each segment was individually addressed by its separate conductive yarns. The segments were actuated in sequence, first with only segment A active, then both A and B, and finally with all three A, B, and C together. The laser scanner recorded the resulting displacement profile, in the bending direction (z-direction), of the entire assembly in each case. The minimum and maximum displacements were extracted, at three places on every segment, at the top, in the middle, and at the bottom (tip).

The displacement profile of the assembly is shown in Figure 9. An increase in curvature on the fabric assembly level is prevalent, as more segments were activated. For example, as A + B + C was active, top segments displayed a reduced range of displacement

in their respective areas, while the overall assembly shifted further left of the center line. This demonstrates that even though actuating segments were only mechanically connected through a few nonactuating weft yarns, this was sufficient in creating an overall interconnected displacement behavior in the fabric during actuation. As more segments were active, the range of displacement of the overall fabric actuator also increased, from 1.94 ± 0.11 mm (A active) to 2.37 ± 0.16 mm (A + B active), and finally 3.91 ± 0.10 mm (A + B + C active), noted as z_1 , z_2 , and z_3 respectively in Figure 8.

3.4 | Lifetime Performance and Application

3.4.1 | Long-Term Actuation of Woven Actuators

Garments or wearable products are beneficial for a range of applications, as they can be administered and used by people in their homes and comfortably worn for a long time. Durability and long-term performance of woven actuators in such applications are therefore of importance. The displacement of woven actuator segments was measured at predetermined intervals: daily for the first

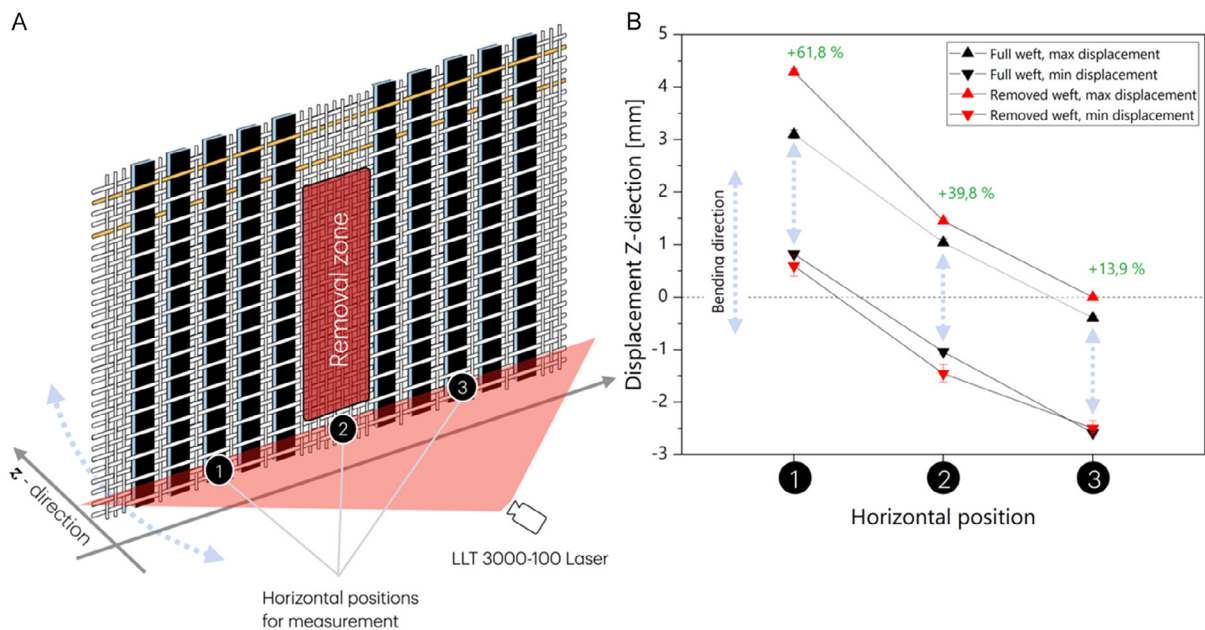


FIGURE 8 | Influence of nonactuating weft yarns in a parallel assembly of woven actuator segments. Displacement is measured across the sample width (warp yarn direction) (A). Before weft yarns are removed (Full_{weft}), the fabric actuator shows even displacement along the three measurement points (B). After weft yarns are removed (Removed_{weft}), the behavior of the fabric actuator changes, showing an increased displacement range and less uniform movement between the width of the actuator.

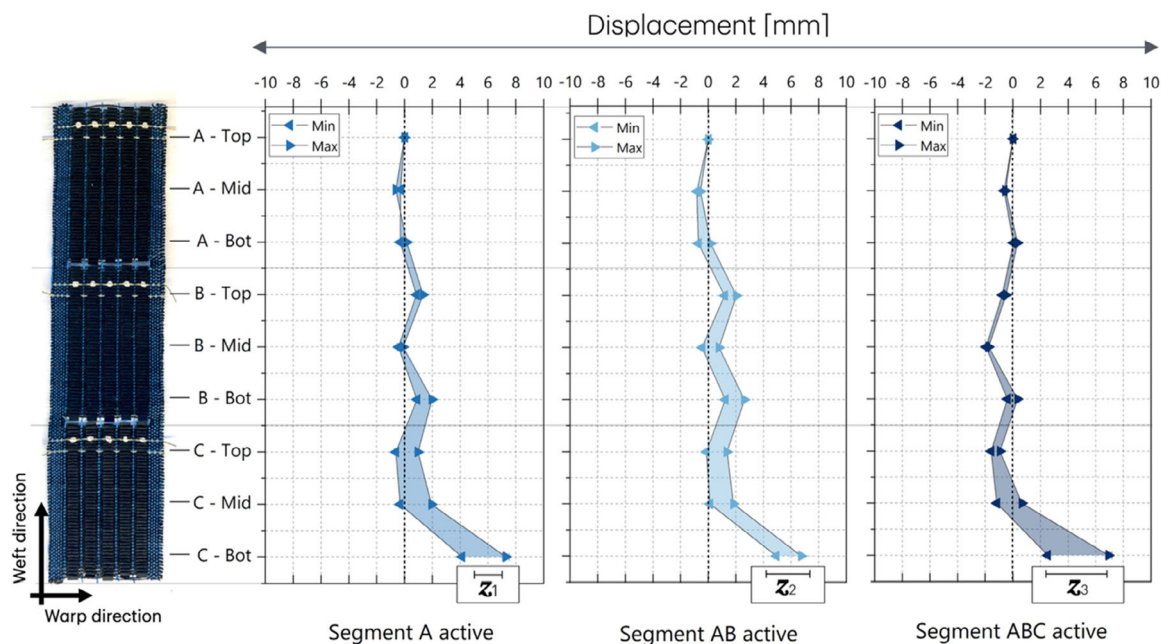


FIGURE 9 | A serial assembly consisting of three segments, A, B, and C which together create an interconnected fabric actuator. Three positions are recorded on each segment and used to evaluate the displacement behavior of the assembly. Min and max displacement at each position, from origin-point 0, is shown where the shaded area represents the range of displacement in the z-direction.

week, and subsequently after 19, 28, 56, and 84 days. Prior to each measurement, each sample underwent 5 precycles, followed by 10 full actuation cycles at ± 2 V for 30 s half-cycle duration. In between each measurement, the samples were kept in sealed sample containers in ambient conditions. As seen in Figure 10, the average displacement was reduced over the course of approximately 3 months. Initial displacement of 6.78 ± 0.11 mm was seen to decline to 5.5–6 mm the first 7 days, then further decline

reaching 1.26 ± 0.58 mm after 84 days. This behavior may stem from material degradation, such as microcracks from mechanical impact of warp yarns due to warp tension (Figure S8) and decrease in electrochemical activity of TYs, indicated by the decline in charge transfer measured during assessment as seen in Figure S9. The redox charge decreased progressively over the course of the 3 months of evaluation, suggesting degradation of the system. The deterioration could be linked to degradation of

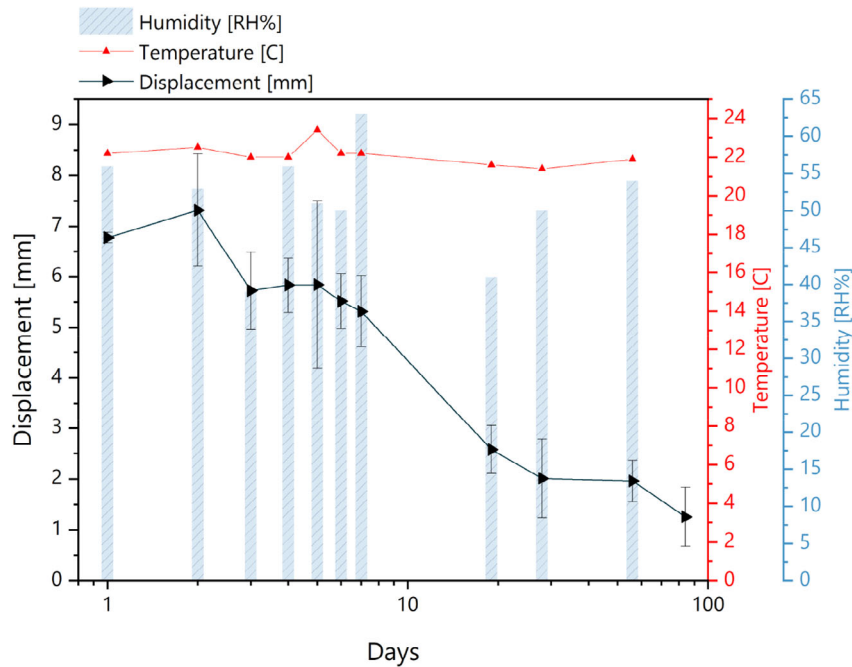


FIGURE 10 | Average displacement of woven segments over the course of 84 days. Displacement was tested every day during the first 7 days, then at lower intervals the following months.

PPy layers due to the higher voltage exposure [47], decreased PVDF membrane integrity, or changes to the IL itself. ILs are known to most often be hygroscopic in nature, where the adsorption of water from the air can influence their physiochemical properties [48]. As such, though the recorded relative humidity is relatively stable during the evaluation period, further experiments to determine its relation to the decline in performance should be done. Furthermore, textiles are porous materials. Absorption of IL is a possibility as warp yarns are in direct contact with the TYs throughout actuation and storage between use. Potential solutions could involve encapsulation of the TYs or optimize warp yarn materials which minimize the risk of IL leakage into the fabric structure.

3.4.2 | Towards On-Body Applications of Woven Actuators

The weaving process allows for the simultaneous assembly of both actuating yarns and conductive yarns to make woven actuators with integrated electrical control. Furthermore, structural, passive yarns support the overall fabric structure and contribute to mechanical stability and comfort properties. Textile actuators therefore become suitable for the development of wearable actuators for on-body applications. As a woven fabric can assemble multiple actuating yarns and exhibit additive force generation (Figure 6) while maintaining conformability to complex shapes, the resulting collective force output can be effectively transferred onto the human body. Figure 11 shows

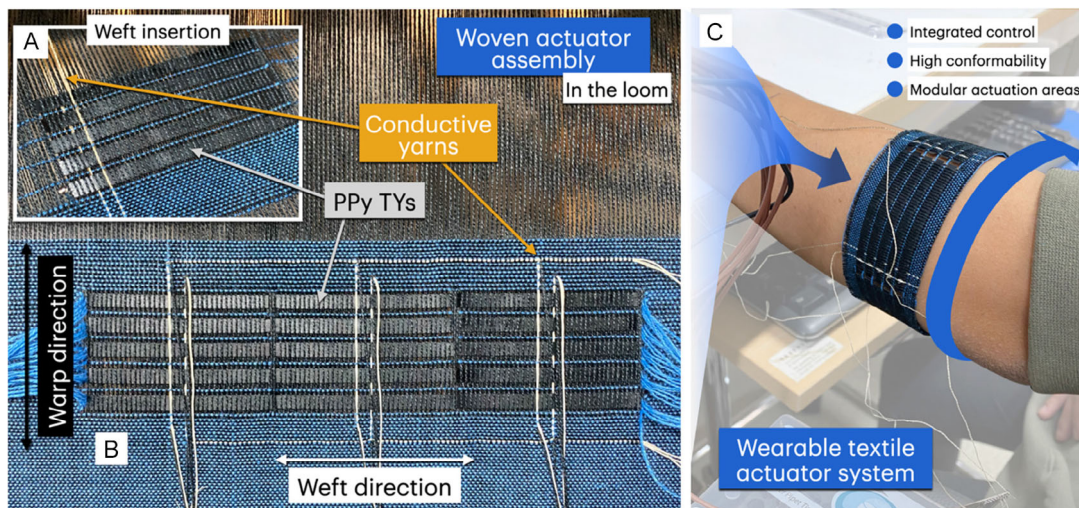


FIGURE 11 | Development of a prototype wearable actuating garment. (A) actuating yarns are integrated through weft insertion. (B) Electrical connections can be added directly in the weaving loom. (C) For on-body applications, woven actuators require a suitable conformal ability, capable of shaping around the body.

how a wearable textile actuator is assembled. In the figure, TYs are seen integrated into the fabric construction (Figure 11A) (15 TYs in total) as three serially connected actuator segments. The conductive pathways have been introduced into the fabric at specific entry and exit locations during the weaving process by switching the conductive yarn position from warp to weft, which enables precise control of their placement. The entirety of the fabric actuator can be addressed simultaneously if yarn paths are integrated together (Figure 11B). However, each segment can be addressed and controlled individually if the conductive yarn pairs are separated (Figure 11C). The placement of conductive yarns can also be adapted to mitigate potential risks with ohmic drop, a common issue for EAP-based actuators [49–52]. However, silver-based conductive materials may result in secondary reaction with the PPy surfaces, as seen in Figure S8C–F. Optimization of chosen materials is crucial for reliability in future fabric actuators based on PPy TY technology. This is a prototype of a wearable actuating garment for haptic applications, which could be complemented by the addition of sensors and powering. Passive materials in the warp and weft could be further exchanged to fulfill different comfort requirements. Two-dimensional actuation, as provided by fabric actuators, has potentially a broad spectrum of applications that include applications where *exercising forces* are central, such as actuators mechanically impacting skin receptors for giving navigation clues for people with blindness or even implementing tactile sign communication; and where *size change* is central, including pore opening membranes and size-selective controlled filters. Furthermore, applications focusing on *stiffness change* include adaptive compression garments and self-mounting packaging materials.

4 | Conclusion

This study demonstrates the construction of reliable, stable, actuating, long-lifetime yarns of a structured TY construction based on a membrane strategy. Actuation is manifested as force exertion and deformation in a bending modality. Comparing different PPy thicknesses and driving voltages together with examining the impact of ILs optimized the bending motion of the TY. By this, textile actuation at the fiber level is demonstrated.

Textile actuation on the fabric level is made possible by weaving TYs into a fabric. The weaving process combined three classes of yarns: actuating, conductive, and passive. Passive yarns contribute to the structural cohesion of the overall fabric materials, which include all yarns in a fabric. Actuating and conductive yarns are both structural and functional. The integration of conductive yarns transforms the woven actuator segments into electrical circuits that can be individually addressed, in total forming a Device. Besides their conductive and actuating function, all yarns contribute structurally to the fabric, where their specific interlacement pattern also determines the mechanical properties of the fabric, in fact defining it as a Material also on a fabric level. Thus, we are demonstrating the “D = M” property of textiles. Meaning that while fabrics are assembled in the weaving loom (becoming a Material), they are simultaneously becoming a Device. Thanks to the woven approach taken, additivity of force

(by parallel arrangement) as well as amplification of displacement (by serial arrangement of actuating TYs) is shown.

Weaving as a process (but not necessarily the very weaving patterning) is in principle agnostic with respect to the actuation mechanism as long as the actuating yarns are processable, i.e., fulfilling strength, abrasion resistance, elasticity, diameter, and length requirements. Thus, other types of actuating yarns could be integrated using weaving too. We also evinced the application of woven actuators as a wearable, on-body haptic device, and by this, demonstrating textiles at the garment level. Thanks to the internal infrastructure of conducting pathways made possible by the weaving patterning, the combination of smaller segments into larger structures, i.e., textiles-within-textiles, is possible. In addition, due to the fact that the actuator is a textile, compliance matching toward the skin is achieved. Likewise, the garment can directly handle the (convex) geometry of the forearm and achieve a close contact necessary for reliable haptic communication. The findings of this study demonstrate the promising application of textiles for the development of wearables and soft robotics.

5 | Experimental Section/Methods

5.1 | Materials

Polyvinylidene fluoride (PVDF) membrane Immobilon-P IPVH00010 was bought from Merck and used as received. Pyrrole (Sigma–Aldrich) was distilled under vacuum and stored at -20°C before use. Choline acetate (Sigma–Aldrich) was used as received, after being left inside an open beaker under the hood overnight. Sodium dodecylbenzenesulfonate (NaDBS, Sigma–Aldrich), 1-ethyl-3-methylimidazolium bis(trifluoromethylsulfonyl)imide (EMIMTFSI, Sigma–Aldrich), lithium bis(trifluoromethanesulfonyl)imide (LiTFSI, Sigma–Aldrich), and propylene carbonate (PC, Sigma–Aldrich) were used as received.

5.2 | Fabrication of PPy/PVDF/PPy TYs

$11 \times 8 \text{ cm}^2$ pieces of polyvinylidene fluoride (PVDF) membrane were cut from a roll of commercial Immobilon-P IPVH00010, washed with isopropanol and water, and dried with pressurized air. Then, a Cr layer was sputtered typically during 45 s at 300 V, 300 mA, 2 mTorr as an adhesion layer, and an Au layer typically during 75 s at 400 V, 250 mA, 4.5 mTorr as a conducting layer. The process was repeated on the other side of the PVDF piece to obtain a conductive coating on both sides of the membrane. Finally, the $11 \times 8 \text{ cm}^2$ was cut into smaller pieces of $5.5 \times 4 \text{ cm}^2$.

Next, PPy was electropolymerized on each of those pieces (connecting both sides so electropolymerization occurred on both sides simultaneously) in a 0.1 M pyrrole, 0.1 M NaDBS aqueous solution at room temperature by applying 0.6 V vs. Ag/AgCl (BASMF2052 from BASi) during enough time to consume 40 C (or a charge density of 1.82 C cm^{-2}) by using a potentiostat/galvanostat AutoLab PGSTAT 204 and Nova 2.1 software (Metrohm). Once the electropolymerization finished, a potential of -0.2 V was applied for 300 s in the same electrolyte. Then, the PPy/PVDF/PPy pieces were immersed in water and washed (by changing the water at least 10 times) for 14 h. Then, these pieces were dried with tissue paper and put into vacuum at room

temperature to dry for 4 h. Finally, the borders of these big pieces were cut with scissors or scalpel, and TYs were cut having dimensions of $50 \times 3 \text{ mm}^2$. These TYs were immersed in the ionic liquid to swell overnight and thereafter left to dry for 3 h before using them.

5.3 | Weaving of Fabric Actuators

A semi-automatic ARM AG CH-3507 BIGLEN weaving loom (Atelier ARM, Switzerland) with 24 shafts was used to assemble the fabric actuators. Warp yarns as well as supporting (nonactuating) weft yarns consisted of black Polyester (Nm 40/2) staple-fiber yarns.

5.4 | Actuation Setup

After drying, electrical connection of individual TYs was done by clamping them with a CR0060 Kelvin Clip which contact pads were covered with Cu tape. These Kelvin Clips allowed for separated connection between the 2 sides of the TYs. Electrical stimulation was applied by using a potentiostat/galvanostat AutoLab PGSTAT 204 and Nova 2.1 software (Metrohm). A similar potentiostat system (Metrohm AG, Switzerland) was used to stimulate and control actuation of woven actuators. Samples were electrically stimulated either by direct clamping by CR0060 Kelvin Clip connectors or addressed using integrated conductive yarns, Liberator 40 ($0.5 \Omega/\text{cm}$), a Vectran multifilament liquid crystal polymer core (LCP), and plated metal (produced by Syscom Technology Inc.). To ensure a secure electrical connection in these samples, conductive silver suspension (AGG3691, Agar Scientific Ltd, UK) was used on the interlacing points between the conductive yarns and the TYs. Textile actuators with integrated circuitry were cantilevered by mechanical clamping, approximately 4 mm in on the sample using a clip with thin plastic sheets, enabling a soft and non-damaging grip. The electrical connections are made using the integrated conductive yarns. In general, each sample was precycled for 5 cycles before taking any measurements, and measurement running over 10 cycles (oxidation and reduction) at $\pm 2\text{V}$ potential set by the potentiostat.

5.5 | Displacement Characterization

The movement of individual TYs was recorded by using a camera VEHO Discovery VMS-004, with mm paper behind the TY actuator. The videos were analyzed by a home-made MATLAB script to measure the displacement of the tip. Displacement of woven actuators was measured using an LLT 3000-100 laser scanner (Micro-Epsilon, Sweden) (Figure S10), with scanCONTROL software to record profile sequences of actuators. From the profile sequence, the positional data was extracted and further analyzed using OriginLab software. The clamping setup was placed in front of a black paper to eliminate background noise during the measurement. The sample is positioned at approximately 270 mm from the laser source point with the laser beam positioned in the middle of the sample, as seen in Figure S10. Extraction of data was generally done at the tip of the sample to gather maximum displacement output, except for samples with multiple actuating areas where further points were extracted.

5.6 | Characterization of Blocking Force

The blocking force exerted by both individual TYs and woven actuators was characterized with the same equipment; a lever arm system (Cambridge Technology Inc. 200B (US)) with servo controller in isometric mode was used, ensuring that the tip of the actuator and the tip of the lever arm were always in contact. The setup was modified slightly for woven actuators, adding a small cross-bar wire attached to the width of the sample to enable a measurement of the overall generated force by the fabrics.

5.7 | Microscopy

The surface of TYs was optically characterized by using an Eclipse Ei R Microscope (Nikon, Japan) at $\times 4$ and $\times 10$ magnification.

Acknowledgments

We thank Hanna Lindholm for assistance in the weaving lab. The authors acknowledge the financial support of the European Union's Horizon 2020 research and innovation program under grant agreement no. 825232 "WEAFING" and Erling-Persson Foundation (grant no 2020-00054 and 2023-0092).

Funding

The authors acknowledge the financial support of the European Union's Horizon 2020 research and innovation program under grant agreement no. (825232) "WEAFING" and Erling-Persson Foundation (grant no 2020-00054 and 2023-0092).

References

1. D. Trivedi, C. D. Rahn, W. M. Kier, and I. D. Walker, "Soft Robotics: Biological Inspiration, State of the Art, and Future Research," *Applied Bionics and Biomechanics* 5 (2008): 99–117, <https://doi.org/10.1080/11762320802557865>.
2. J. Kim, J. W. Kim, H. C. Kim, L. Zhai, H.-U. Ko, and R. M. Muthoka, "Review of Soft Actuator Materials," *International Journal of Precision Engineering and Manufacturing* 20 (2019): 2221–2241, <https://doi.org/10.1007/s12541-019-00255-1>.
3. A. Chen, R. Yin, L. Cao, C. Yuan, H. K. Ding, and W. J. Zhang, *Soft robotics: Definition and research issues*, in: *2017 24th International Conference on Mechatronics and Machine Vision in Practice (M2VIP)* (IEEE, 2017), 366–370, <https://doi.org/10.1109/M2VIP.2017.8267170>.
4. D. Rus and M. T. Tolley, "Design, Fabrication and Control of Soft Robots," *Nature* 521 (2015): 467–475, <https://doi.org/10.1038/nature14543>.
5. Y. She, S. Song, H.-J. Su, and J. Wang, "A Comparative Study on the Effect of Mechanical Compliance for a Safe Physical Human–Robot Interaction," *Journal of Mechanical Design* 142 (2020): 063305, <https://doi.org/10.1115/1.4046068>.
6. N.-K. Persson, J. G. Martinez, Y. Zhong, A. Maziz, and E. W. H. Jager, "Actuating Textiles: Next Generation of Smart Textiles," *Advanced Materials Technologies* 3 (2018): 1700397, <https://doi.org/10.1002/admt.201700397>.
7. J. Pu, K. Ma, Y. Luo, et al., "Textile Electronics for Wearable Applications," *International Journal of Extreme Manufacturing* 5 (2023): 042007, <https://doi.org/10.1088/2631-7990/ace66a>.
8. A. Tejo Otero, I. Buj Corral, F. Fenollosa, and I. Artés, *Mimicking Soft Living Tissues for 3D Printed Surgical Planning Prototypes Using Additive*

- Manufacturing Technologies*. (Universitat Politècnica de Catalunya, 2021), <https://doi.org/10.5821/dissertation-2117-414264>.
9. V. Sanchez, C. J. Walsh, and R. J. Wood, "Textile Technology for Soft Robotic and Autonomous Garments," *Advanced Functional Materials* 31 (2021): 6, <https://doi.org/10.1002/adfm.202008278>.
10. T. F. Otero and J. G. Martínez, *Conducting Polymers as EAPs: Fundamentals and Materials, Electromechanically Active Polymers*. In: F. Carpi, 237–255 (Cham: Springer International Publishing, 2016), https://doi.org/10.1007/978-3-319-31530-0_11.
11. D. Melling, J. G. Martínez, and E. W. H. Jager, "Conjugated Polymer Actuators and Devices: Progress and Opportunities," *Advanced Materials (deerfield Beach, Fla.)* 31 (2019): 1808210, <https://doi.org/10.1002/adma.201808210>.
12. F. Carpi, R. Kornbluh, P. Sommer-Larsen, and G. Alici, "Electroactive Polymer Actuators as Artificial Muscles: Are They Ready for Bioinspired Applications?," *Bioinspiration & Biomimetics* 6 (2011): 045006, <https://doi.org/10.1088/1748-3182/6/4/045006>.
13. J. D. Madden, P. G. Madden, and I. W. Hunter, *Conducting Polymer Actuators as Engineering Materials*. In: Y. Bar-Cohen, 176–190 (2002), <https://doi.org/10.1117/12.475163>.
14. Y. Bar-Cohen, *Electroactive Polymers as Actuators, in: Advanced Piezoelectric Materials*. 287–317 (Elsevier, 2010), <https://doi.org/10.1533/9781845699758.1.287>.
15. A. Maziz, A. Concas, A. Khaldi, J. Ståhlhand, N.-K. Persson, and E. W. H. Jager, "Knitting and Weaving Artificial Muscles," *Science Advances* 3 (2017): e1600327, <https://doi.org/10.1126/sciadv.1600327>.
16. Y. Wu, Y. Yang, C. Li, Y. Li, and W. Chen, "Flexible and Electroactive Textile Actuator Enabled by PEDOT: PSS/MOF-Derivative Electrode Ink," *Frontiers in Bioengineering and Biotechnology* 8 (2020): 212.
17. C. Backe, J. G. Martínez, L. Guo, C. Plesse, E. W. H. Jager, and N.-K. Persson, "In-Air, Textile Actuators by Conjugated Polymers and Solid-State Electrolyte Tape Yarns," *Advanced Intelligent Systems* 7(2025): 2400629, <https://doi.org/10.1002/aisy.202400629>.
18. K. Gilday, I. Zubak, A. Raabe, and J. Hughes, "From Rigid to Soft Robotic Approaches for Neuroendoscopy," *Advanced Robotics Research* (2025): e202500017, <https://doi.org/10.1002/adrr.202500017>.
19. W. Feng, D. Liu, and D. J. Broer, "Functional Liquid Crystal Polymer Surfaces with Switchable Topographies," *Small Structures* 2 (2021): 1, <https://doi.org/10.1002/sstr.202000107>.
20. S. Baurley, P. Brock, E. Geelhoed, and A. Moore, Communication-Wear: User Feedback as Part of a Co-Design Process, *Haptic and Audio Interaction Design*, eds. I. Oakley and S. Brewster, 56–68 (Springer Berlin Heidelberg, 2007), https://doi.org/10.1007/978-3-540-76702-2_7.
21. C. Thalman and P. Artemiadis, "A Review of Soft Wearable Robots that Provide Active Assistance: Trends, Common Actuation Methods, Fabrication, and Applications," *Wearable Technologies* 1 (2020): e3, <https://doi.org/10.1017/wtc.2020.4>.
22. D. K. Patel, K. Zhong, H. Xu, M. F. Islam, and L. Yao, "Sustainable Morphing Matter: Design and Engineering Practices," *Advanced Materials Technologies* 8 (2023): 2300678, <https://doi.org/10.1002/admt.202300678>.
23. B. Gaihare, G. Alici, G. M. Spinks, and J. M. Cairney, "Effect of Electrolyte Storage Layer on Performance of PPy-PVDF-PPy Microactuators," *Sensors and Actuators B: Chemical* 155 (2011): 810–816, <https://doi.org/10.1016/j.snb.2011.01.053>.
24. K. Rohtlaid, G. T. M. Nguyen, C. Soyer, E. Cattani, F. Vidal, and C. Plesse, "Poly(3,4-Ethylenedioxythiophene): Poly(styrene Sulfonate)/ Polyethylene Oxide Electrodes with Improved Electrical and Electrochemical Properties for Soft Microactuators and Microsensors," *Advanced Electronic Materials* 5 (2019): 1800948, <https://doi.org/10.1002/aelm.201800948>.
25. A. Maziz, C. Plesse, C. Soyer, et al., "Demonstrating kHz Frequency Actuation for Conducting Polymer Microactuators," *Advanced Functional Materials* 24 (2014): 4851–4859, <https://doi.org/10.1002/adfm.201400373>.
26. S. Aziz, J. G. Martínez, B. Salahuddin, N. Persson, and E. W. H. Jager, "Fast and High-Strain Electrochemically Driven Yarn Actuators in Twisted and Coiled Configurations," *Advanced Functional Materials* 31 (2021): 10, <https://doi.org/10.1002/adfm.202008959>.
27. S. Mehraeen, M. Asadi, J. G. Martínez, N. Persson, J. Ståhlhand, and E. W. H. Jager, "Effect of Core Yarn on Linear Actuation of Electroactive Polymer Coated Yarn Actuators," *Advanced Materials Technologies* 8 (2023): 2300460, <https://doi.org/10.1002/admt.202300460>.
28. T. F. Otero and J. G. Martínez, "Electro-Chemo-Biomimetics from Conducting Polymers: Fundamentals, Materials, Properties and Devices," *Journal of Materials Chemistry B* 4 (2016): 2069–2085, <https://doi.org/10.1039/C6TB00060F>.
29. R. Shi, F. Pan, and X. Ji, "Soft Actuators Integrated with Control and Power Units: Approaching Wireless Autonomous Soft Robots," *Advanced Robotics Research* (2025): e202500107, <https://doi.org/10.1002/adrr.202500107>.
30. T. F. Otero and E. De Larreta, "Electrochemical Control of the Morphology, Adherence, Appearance and Growth of Polypyrrole Films," *Synthetic Metals* 26 (1988): 79–88, [https://doi.org/10.1016/0379-6779\(88\)90337-2](https://doi.org/10.1016/0379-6779(88)90337-2).
31. T. F. Otero and C. Santamaría, "Dependence of Polypyrrole Production on Potential," *Synthetic Metals* 51 (1992): 313–319, [https://doi.org/10.1016/0379-6779\(92\)90285-Q](https://doi.org/10.1016/0379-6779(92)90285-Q).
32. F. García-Córdova, L. Valero, Y. A. Ismail, and T. F. Otero, "Biomimetic Polypyrrole Based All Three-in-One Triple Layer Sensing Actuators Exchanging Cations," *Journal of Materials Chemistry* 21 (2011): 17265–17272, <https://doi.org/10.1039/C1JM13374H>.
33. T. F. Otero and J. M. Sansiñena, "Bilayer Dimensions and Movement in Artificial Muscles," *Bioelectrochemistry and Bioenergetics* 42 (1997): 117–122, [https://doi.org/10.1016/S0302-4598\(96\)05112-4](https://doi.org/10.1016/S0302-4598(96)05112-4).
34. T. F. Otero and J. G. Martínez, "Artificial Muscles: A Tool To Quantify Exchanged Solvent during Biomimetic Reactions," *Chemistry of Materials: A Publication of the American Chemical Society* 24 (2012): 4093–4099, <https://doi.org/10.1021/cm302847r>.
35. N. Aydemir, P. A. Kilmartin, J. Travas-Sejdic, et al., "Electrolyte and Solvent Effects in PPy/DBS Linear Actuators," *Sensors and Actuators B: Chemical* 216 (2015): 24–32, <https://doi.org/10.1016/j.snb.2015.03.098>.
36. R. Kiefer, P. A. Kilmartin, G. A. Bowmaker, R. P. Cooney, and J. Travas-Sejdic, "Actuation of Polypyrrole Films in Propylene Carbonate Electrolytes," *Sensors and Actuators B: Chemical* 125 (2007): 628–634, <https://doi.org/10.1016/j.snb.2007.03.008>.
37. M. Luberti, C. Olkis, G. Bensted, and G. Santori, "Water Sorption Equilibrium on 2-Hydroxyethyl-Trimethylammonium Acetate in the Temperature range 298.25–349.55K," *Fluid Phase Equilibria* 522 (2020): 112758, <https://doi.org/10.1016/j.fluid.2020.112758>.
38. A. Kaur, S. Bansal, D. Chauhan, K. K. Bhasin, and G. R. Chaudhary, "The Study of Molecular Interactions of Aqueous Solutions of Choline Acetate at Different Temperatures," *Journal of Molecular Liquids* 286 (2019): 110878, <https://doi.org/10.1016/j.molliq.2019.110878>.
39. L. Bay, T. Jacobsen, S. Skaarup, and K. West, "Mechanism of Actuation in Conducting Polymers: Osmotic Expansion," *The Journal of Physical Chemistry. B* 105 (2001): 8492–8497, <https://doi.org/10.1021/jp003872w>.
40. T. F. Otero and M. Alfaro, "Oxidation Kinetics of Polypyrrole Films: Solvent Influence," *Journal of Electroanalytical Chemistry* 777 (2016): 108–116, <https://doi.org/10.1016/j.jelechem.2016.07.043>.
41. G. Alici, P. Metz, and G. M. Spinks, "A Methodology Towards Geometry Optimization of High Performance Polypyrrole (PPy)

Actuators,” *Smart Materials and Structures* 15 (2006): 243–252, <https://doi.org/10.1088/0964-1726/15/2/003>.

42. T. F. Otero and J. G. Martinez, “Activation Energy for Polypyrrole Oxidation: Film Thickness Influence,” *Journal of Solid State Electrochemistry : Current Research and Development in Science and Technology* 15 (2011): 1169–1178, <https://doi.org/10.1007/s10008-010-1170-1>.

43. D. Melling, S. Wilson, and E. W. H. Jager, “The Effect of Film Thickness on Polypyrrole Actuation Assessed Using Novel Non-Contact Strain Measurements,” *Smart Materials and Structures* 22 (2013): 104021, <https://doi.org/10.1088/0964-1726/22/10/104021>.

44. I. Villarreal, E. Morales, T. F. Otero, and J. L. Acosta, “Electropolymerization Kinetics of Pyrrole in Aqueous Solution on Graphite Felt Electrodes,” *Synthetic Metals* 123 (2001): 487–492, [https://doi.org/10.1016/S0379-6779\(01\)00343-5](https://doi.org/10.1016/S0379-6779(01)00343-5).

45. E. Smela, “Microfabrication of PPy Microactuators and Other Conjugated Polymer Devices,” *Journal of Micromechanics and Microengineering : Structures, Devices, and Systems* 9 (1999): 1–18, <https://doi.org/10.1088/0960-1317/9/1/001>.

46. I. J. Suarez, T. F. Otero, and M. Marquez, “Diffusion Coefficients in Swelling Polypyrrole: ESCR and Cottrell Models,” *The Journal of Physical Chemistry B* 109 (2005): 1723–1729, <https://doi.org/10.1021/jp046051q>.

47. T. W. Lewis, G. M. Spinks, G. G. Wallace, A. Mazzoldi, and D. De Rossi, “Investigation of the Applied Potential Limits for Polypyrrole when Employed as the Active Components of a Two-Electrode Device,” *Synthetic Metals* 122, no. 2 (2001): 379–385, [https://doi.org/10.1016/S0379-6779\(00\)00397-0](https://doi.org/10.1016/S0379-6779(00)00397-0).

48. I. F. D. Francesco, N. Calisi, M. Creatini, B. Melai, P. Salvo, and C. Chiappe, “Water Sorption by Anhydrous Ionic Liquids,” *Green Chemistry : an International Journal and Green Chemistry Resource : Gc* 13, no. 7 (2011): 1712, <https://doi.org/10.1039/c1gc15080d>.

49. P. G. A. Madden, J. D. W. Madden, P. A. Anquetil, N. A. Vandesteeg, and I. W. Hunter, “The Relation of Conducting Polymer Actuator Material Properties to Performance,” *IEEE Journal of Oceanic Engineering* 29 (2004): 696–705, <https://doi.org/10.1109/JOE.2004.833139>.

50. G. Alici, A. Punning, and H. R. Shea, “Enhancement of Actuation Ability of Ionic-Type Conducting Polymer Actuators Using Metal Ion Implantation,” *Sensors and Actuators B: Chemical* 157 (2011): 72–84, <https://doi.org/10.1016/j.snb.2011.03.028>.

51. S. V. Ebadi, H. Fashandi, D. Semnani, B. Rezaei, and A. Fakhrali, “Overcoming the Potential Drop in Conducting Polymer Artificial Muscles through Metallization of Electrospun Nanofibers by Electroplating Process,” *Smart Materials & Structures* 29 (2020): 085036, <https://doi.org/10.1088/1361-665X/ab98ed>.

52. S. Dutta, S. Mehraeen, N.-K. Persson, J. G. Martinez, and E. W. H. Jager, “The Effect of Electroactive Length and Intrinsic Conductivity on the Actuation Behaviour of Conducting Polymer-Based Yarn Actuators for Textile Muscles,” *Sensors and Actuators B: Chemical* 370 (2022): 132384, <https://doi.org/10.1016/j.snb.2022.132384>.

Supporting Information

Additional supporting information can be found online in the Supporting Information section. **Supporting Fig. S1:** Overview of parallel and serial assembly of woven segments into multi-functional woven actuators.

Supporting Fig. S2: (A) Au coated PVDF membrane, (B) big piece of PPy coated Au coated PVDF membrane, (C) smaller piece of PPy coated Au coated PVDF membrane, and (D) 5 cm long TY. **Supporting Fig. S3:** (a) Electropolymerization of PPy by applying a constant potential of +0.6 V to a Au coated PVDF membrane until a charge of 40 C was consumed; and (b) cyclic voltammetry obtained from a PPy/PVDF/PPy trilayer at 20 mV s⁻¹ after filling the PVDF membrane with choline acetate.

Supporting Fig. S4: Force exerted by the tip of a PPy/PVDF/PPy TY, obtained by the consumption of 40C during electropolymerization of PPy, by applying square potential waves of ±1.0 V, each potential kept

for 60 s. **Supporting Fig. S5:** Displacement and blocking force of individual TYs tested at HB. At ±2 V, 30s half-cycle time. **Supporting Fig. S6:** Order of activation in a sequential activation strategy for testing additivity of force inside a woven actuator consisting of 5 TYs. **Supporting Fig. S7:** Sample structure of woven segments with different number of TY units integrated (1-5 TYs). Each unit contains one TY and three picks (weft yarns) of non-actuating PES yarns on each side. **Supporting Fig. S8:** Microscopy of TYs after removal from woven fabric structure. (A) shows an area in the center of the middle segment of the TY surface. In contrast, (B) shows micro-fractures at the edge of the TY most likely caused by perpendicular warp yarns as they cross between face and back of the fabric structure in the woven construction, causing PVDF membrane particles to also become loose. Traces of contact points after removing conductive yarns is also visible, where (C) silver suspension is attached to the TY surface or (D) showing potentially secondary reactions. Furthermore, this effect is present at some of the edges as well (E,F). **Supporting Fig. S9:** Mean charge evolution for three samples during age testing (charge data extracted from each sample’s three last cycles), illustrated during +/–2V square wave potentials. **Supporting Fig. S10:** Laser scanner measurement setup. Using an LLT 3000-100 laser scanner and scanCONTROL software the samples’ bending profiles could be recorded and analyzed.